ADVANCED OPTICAL MATERIALS
www.advopticalmat.de

Real-Time Detection of Coherent Vibrational Dynamics in TiN Films

*Andrea Iudica, Silvia Rotta Loria, Cristina Mancarella, Luca Mascaretti, Alberto Naldoni, Giulio Cerullo, Andrea Li Bassi, and Margherita Zavelani-Rossi**

Titanium nitride (TiN) has recently gained considerable interest because of its remarkable plasmonic properties and for its strong electron–phonon (e–ph) coupling, leading to extremely fast (<100 fs) electron-lattice cooling. Here, the generation of coherent phonons in TiN films is reported, along with their real-time detection by means of broadband transient reflection spectroscopy with sub-15-fs temporal resolution. The measurements show damped oscillations, superimposed to excited state electronic decay. A coherent vibrational mode is revealed, with ≈10 THz frequency ascribed to defect-activated normal modes, consistent with spontaneous Raman scattering data, and a dephasing time of ≈250 fs. Two π-phase flips are also observed located at photon energies corresponding to interband optical transitions (at 3.2 and 2.5 eV), ascribed to selective coupling of the vibrational mode to these transitions; the energy modulation induced by the vibrational coherence is evaluated. It is shown that the displacive excitation of coherent phonons model describes the coherent response in terms of temporal behavior and of spectral amplitude profile. Overall, a comprehensive and detailed analysis of coherent phonons in TiN films, so far undected, is provided and relevant information on TiN photo-physical properties, potentially useful for its applications, is given.

1. Introduction

Titanium nitride (TiN) is one of the most prominent members of the refractory transition metal nitrides family. It is characterized by a high melting point, good thermal, and electrical conductivities and chemical stability. These characteristics made it largely used as a coating material in industrial applications. Moreover, they make it very appealing for electronics, in particular for complementary metal oxide semiconductor (CMOS) devices.[1,2] Owing to its prominently metallic behavior, given by the presence of an unusually high free electron density within its conduction band, TiN exhibits also very interesting optical properties and it is nowadays emerging as a promising novel plasmonic material.[1] TiN can have superior performances compared to traditional noble metals. In addition to the already mentioned outstanding mechanical, chemical, and temperature durability, other advantages of TiN consist in the possibility to tune the optical constants at the synthesis stage by stoichiometry control, tailoring the spectral position of the plasmonic resonance in the visible and near-infrared (NIR) range (much more than conventional metals), together with its extremely low absorption losses in the same spectral range.[1–6] This paves the way to the implementation of novel functionalities and new photonic devices.[6,7] TiN has been exploited for example in solar-thermal conversion, on chip applications[8–11] and water splitting.[12]

A. Iudica, S. Rotta Loria, G. Cerullo
Dipartimento di Fisica
Politecnico di Milano
Piazza Leonardo da Vinci, 32, Milano I-20133, Italy
C. Mancarella, A. Li Bassi, M. Zavelani-Rossi
Dipartimento di Energia
Politecnico di Milano
Via G. Ponzio 34/3, Milano I-20133, Italy
E-mail: margherita.zavelani@polimi.it

The ORCID identification number(s) for the author(s) of this article can be found under https://doi.org/10.1002/adom.202401390

DOI: 10.1002/adom.202401390

L. Mascaretti
Department of Laser Physics and Photonics
Faculty of Nuclear Sciences and Physical Engineering
Czech Technical University in Prague
Běhová 7, Prague 11519, Czech Republic
A. Naldoni
Dipartimento di Chimica and NIS
Università di Torino
Torino 10125, Italy
G. Cerullo, M. Zavelani-Rossi
Istituto di Fotonica e Nanotecnologie (IFN-CNR)
Piazza L. da Vinci 32, Milano 20133, Italy

The optical properties of TiN are interesting both in the static and in the transient domain. While the optical response in the static regime has been widely studied so far,[4,13] the transient regime has been investigated only very recently.[14–17] These time-resolved studies have shown that after photo-excitation and hot electron generation, the thermalization of the hot electrons with the lattice is extremely fast (<100 fs), one order of magnitude faster than e.g., in gold (≈1 ps).[14] Moreover, it has been shown that the transient response can be tuned by varying the fabrication parameters, in conjunction with the tuning of static properties.[17] The giant ultrafast optical response has been explained through the interband and intraband contributions to the modulation of the TiN permittivity, with the interband part dominating in the first ≈150 fs.[17] The ultrafast relaxation is governed by a strong e–ph (e–ph) coupling.

Together with several other transition metal carbides (TMCs) and nitrides (TMNs), TiN is a well-known conventional superconductor with a relatively high critical temperature, whose behavior is fully understood in terms of the Bardeen-Cooper-Schrieffer (BCS) theory.[18] Recently, the energy value of the superconducting gap has been determined through tunnel conductance measurements.[19] A peculiar fingerprint of the effect of strong e–ph coupling in this material and other similar superconducting TMCs and TMNs is found in the phonon dispersion relation. In particular, a set of phonon anomalies in the acoustic branches is observed in several points of the Brillouin Zone (BZ), specifically around the K, L, and X points.[18,20] Several works[21,22] identified the origin of this feature in a resonance-like increase in the nonlocal dielectric function at the Fermi level E_F, due to the hybridization of metallic $d(T_{2g})$ states and non-metal p states. The sudden change in the electron screening of the internuclear interaction leads to a set of Kohn-like anomalies at wavevectors satisfying the Fermi nesting condition. Interestingly, it is found from strong coupling theory that this effect is linked to the unusually high critical superconducting temperature T_c of TMNs and TMCs.

A detailed understanding of the phononic behavior of TiN would thus be important for the complete characterization of the material. Raman spectroscopy and IR-absorption spectroscopy have been long established as the staple techniques for determining the characteristic vibrational modes of the ground state. Nevertheless, these techniques operate in the frequency domain and thus give limited information on the vibrational modes; in particular they fail in providing a complete description of the oscillations that includes the amplitude, the phase and the dephasing time. Moreover, they operate in the ground state, and cannot access the information of the dynamics of out-of-equilibrium states in a time-resolved fashion. To directly observe the vibrational dynamics, one can use direct or indirect impulsive excitation of coherent lattice motion by an ultrafast laser pulse and then study the out-of-equilibrium response in the time-domain, thus providing all information complementary to Raman measurements. This method has proven to be a powerful and rich approach to investigate the properties of matter and has been applied to a variety of materials (see recent reviews).[23,24] Coherent phonon spectroscopy is based on time-resolved transient absorption (TA) or reflection (TR) techniques with ultrashort laser pulses, with duration lower than half of the period of oscillations to be studied (typically 10–100 fs), where a normal mode of a material can be driven directly (i.e., with light pulses in the MIR-THz range, in resonance with the targeted vibrational mode), as was recently done for high temperature superconductors, antiferromagnetic compounds, or strongly correlated materials,[25–28] or by other indirect schemes. The most well studied case in the latter category is the one where a light pulse drives intra- or inter-band electronic transitions, which then trigger vibrational coherence by means of e–ph coupling. This electron-mediated process is particularly useful in understanding the coupling of single- or multi-particle excitations with phonons, such as for e–ph or exciton-phonon coupling, respectively. Such experiments provided useful insight on novel materials such as mono- and few- layer materials,[29,30] charge density wave materials,[31,32] perovskites,[33–35] to cite a few. The analysis of vibrational coherences allows to disclose their generation mechanisms and e–ph coupling interaction characteristics. To this purpose, several phenomenological models have been proposed to pinpoint the physical mechanism at the origin of coherent phonon generation. Namely, impulsive stimulated Raman scattering (ISRS)[36] and displacive excitation of coherent phonons (DECP)[37] models were proposed, depending on the virtual or real nature of the electronic excited state. Although the physical depiction of these two mechanisms is different, it was shown that they can be incorporated in a unified framework, taking into account both virtual and real electronic transitions by means of a complex Raman tensor.[38,39]

Overall, these results shed light into fundamental physical processes and open the route to technological applications. In particular, control of coherent modulations of the optical properties could be exploited for the fabrication of optoelectronic devices operating via collective lattice motion, as proposed for high-speed actuators, transducers and sensors,[40–43] which can be operated at extremely high frequencies (up to several THz[44,45]). In this context, the detection of coherent phonons of TiN is interesting yet challenging, as it requires a pulse duration lower than 50 fs, together with broad UV–vis spectral range.

In this work, we perform ultrafast TR spectroscopy on polycrystalline TiN films with sub-15 fs temporal resolution, and achieve the first-time detection of a coherent vibrational mode in this material. We identify its coupling to the electronic states and optical transitions by analyzing the phase and amplitude profile over the wide probe spectral range. We postulate the coherent mode to be originated by the coupling of photoexcited hot carriers within the conduction band (CB) with the lattice. We motivate our findings by modeling our experimental data with the DECP formalism, and rule out non-resonant mechanisms such as ISRS. Overall, we provide a detailed phenomenological characterization of the coherent vibrational response in this material, which might prove useful for fundamental physics or further technological applications.

2. Results

2.1. Optical Stationary Properties

The TiN film used in the experiments was fabricated via pulsed laser deposition (PLD) in high vacuum, so as to ensure high compactness and smoothness.[46] The morphology is assessed through scanning electron microscopy (SEM), displaying a nanocrystalline structure and columnar growth (**Figure 1c**), with a thickness of 193 nm. The reflectance and absorbance spectra,

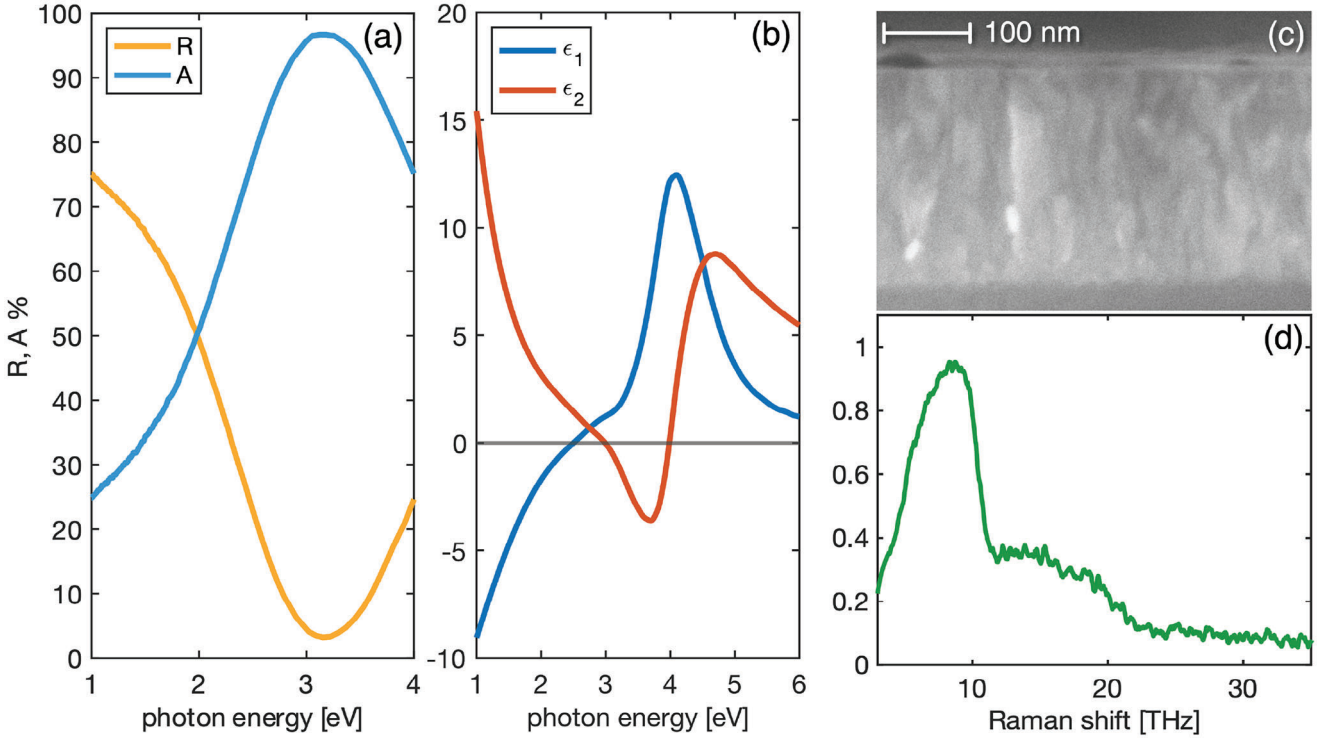

Figure 1. a) Reflectance (yellow line) and absorbance (blue line) spectra of the TiN sample. b) Real (ε_1, blue line) and imaginary (ε_2, red line) part of the pseudodielectric constant of the sample, retrieved from spectrometric ellipsometry. c) Transversal SEM micrograph of the PLD-deposited TiN film. d) Spontaneous Raman spectrum of the TiN sample.

retrieved from standard UV–vis spectroscopy in reflectance configuration, are reported in Figure 1a. The absorption spectrum is characterized by a broad peak, centered at $h\nu = 3.25$ eV. Given the metallic character of TiN, the reflectance spectrum is complementary to absorption, thus exihibiting a dip around the same wavelength, followed by a high reflectance region towards the vis–NIR range. Spectrometric ellipsometry data are used to evaluate the optical constant, ε_1 and ε_2 real and imaginary part respectively, of the pseudodielectric constant of the sample (Figure 1b). The real dielectric constant displays a screened plasma energy of $h\nu_p = 2.5$ eV. The negative-valued dip in ε_2 around 3–4 eV, and the corresponding peak in ε_1 are likely due to Fabry-Pérot resonance caused by a thin (<20 nm) partially oxidized layer (see Figure 1c). In order to take into account this effect, we model the partially oxidized layer as a thin film of TiO_2 and we fit the ellipsometric data by employing the transfer matrix formalism to the optical bilayer (TiN film and TiO_2). In particular, we employ a Drude model with one Lorentz oscillator for the TiN film, and a Tauc-Lorentz oscillator for the oxidized overlayer (further details are provided in the Supporting Information), thus retrieving the dielectric function of TiN exclusively. Relevant information concerning the crystalline order and the vibrational properties of the TiN sample are also provided by spontaneous Raman scattering data, reported in Figure 1d. Indeed, according to the standard Raman selection rules derived from group theory, TiN should be Raman-inactive, since it belongs to the $Fm\bar{3}m$ space group.[47] Nevertheless, a first-order and second-order Raman scattering is allowed due to the unavoidable presence of defects (especially *nitrogen* vacancies), which locally break the lattice symmetry and relax the Raman selection rules.[48–50] This allows for the detection of a set of featureless, broad peaks from the entire BZ, including normally Raman inactive vibrational modes, and from all phonon branches, including the longitudinal acoustic (LA) and transverse acoustic (TA). As illustrated in Figure 1d, the strongest Raman band is located below 10 THz, in a frequency range occupied exclusively by LA and TA modes.[47] The qualitative aspect of the Raman spectrum can also give an approximate indication of the nonstoichiometry of the TiN film. In particular, according to the literature,[47,51,52] a high ratio between the peaks of the acoustic and optical bands, as in our sample, is typical of a nitrogen deficient structure.

2.2. Transient Time-Resolved Spectroscopy

The ultrafast optical response of TiN is investigated through TR spectroscopy, by time-resolved broadband pump-probe (PP) technique with <15 fs time resolution. The pump photon energy is set at 2.14 eV, sufficiently far from the strongest resonant (interband) absorption edges of TiN, which are mostly located in the UV range.[1,4] In this condition, the dominant photoexcitation mechanism is the intraband excitation of free electrons in the vicinity of the Fermi level.[53–55] The following redistribution of the electronic population, characterized by cascaded events of electron–electron and e–ph scattering, induces an ultrafast modulation of the optical properties. It has been very recently shown that in TiN impulsive excitation of free carriers affects the cross-section of both direct (interband) and indirect (intraband)

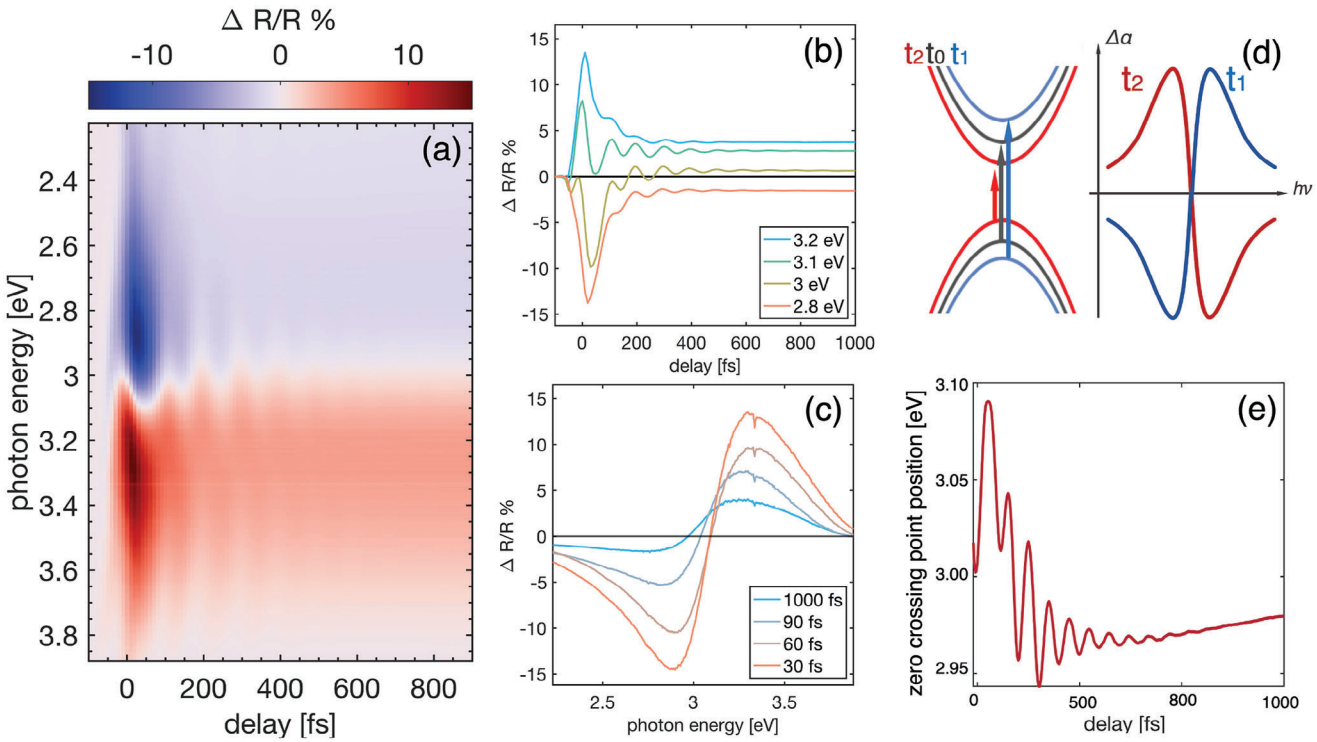

Figure 2. Experimental TR data of the PLD-deposited TiN film. a) Pump-probe map, reporting the transient reflectivity data $\Delta R/R$ % over the entire probe range, at varying delays between pump and probe pulses. b) Dynamics extracted from the TR map at given probe photon energies (indicated in the legend). The signal is characterized by an incoherent decay, superimposed to a set of coherent oscillations lasting less than 1 ps. c) TR spectra extracted from the map at selected delays (indicated in the legend). d) Conceptual, two-band scheme of the phonon-induced modulation in binding energy, and its effect on the absorption coefficient α. For instance, the blueshift of optical absorption in t_1 will correspond to a decrease of the absorption coefficient α at energies lower than the equilibrium photon energy and viceversa. e) Temporal evolution of the zero-crossing point.

transitions, as discussed in Ref. [17]. **Figure** 2a,b,c display the experimental data as normalized TR $\Delta R/R$, where $\Delta R = (R_{ON} - R_{OFF})$ is the difference between the reflectivity after excitation (ON) and without excitation (OFF), and is normalized over R_{OFF}. In the analysis of the TR data, the presence of a partially oxidized layer on the surface of TiN (as mentioned in the previous section) can be neglected. This is motivated by the high transparency of TiO_2 in the photon energy range of the pump pulse and by the relatively low estimated thickness of such overlayer. Transient transmission measurements on a 200-nm-thick TiO_2 film (Figure S1, Supporting Information) confirm this hypothesis and are in perfect agreement with previous works on time resolved spectroscopy on metallic TiN,[15,17] thus ensuring that the TR signal is solely attributable to the TiN film.

The TR signal displays a derivative lineshape that corresponds to a red shift of the reflectivity spectrum, with peaks/dips of opposite sign: one positive at photon energies higher than ≃3.1 eV and one negative at lower photon energies (see Figure 2a,c). The TR dynamics (Figure 2b) are characterized by a fast response with an instantaneous rise and a fast decay lasting 80 fs, followed by a very slow decay (on a time scale much longer than the temporal delay range investigated). This behavior is ascribed to fast relaxation of the nonthermal electron population via electron–electron scattering, occurring on a timescale faster than the time resolution of the experiment, followed by relaxation through a process of e–ph scattering taking place in less than 100 fs and lastly phonon–phonon scattering events, requiring much longer times (generally more than one nanosecond).[56] The modulation of the interband transition cross-section is responsible for the most of the optical response within the first picosecond.[17]

As explained below, we ascribe the oscillations to the excitation of coherent vibrational modes in the sample. By fitting the incoherent dynamics related to the hot carrier relaxation (details in the Experimental section), we isolate the residuals, which are found to be solely corresponding to the coherent dynamics, and are shown in **Figure** 3a. We notice clear oscillatory dynamics lasting approximately 1 ps, with two phase flips in the oscillations, located at approximately 3.3 and 2.5 eV. In order to resolve the probe photon energy dependence of the frequency, amplitude, and phase profile of the coherent mode being excited, we perform a Fast Fourier Transform (FFT) of the residuals over the entire probe range (as reported in Figure 3b).

Figure 3b shows the intensity of the FFT as a function of the frequency and of the probe photon energy; each line of this map corresponds to the FFT of the corresponding line of the residuals map shown in Figure 3a. One vibrational mode at ≈10 THz appears, at all probe wavelengths, with a varying amplitude profile across the spectrum of the probe. More in detail, **Figure** 4a displays the FFT intensity as a function of the oscillation frequency for a probe photon energy of 2.64 eV, from Figure 3b, with

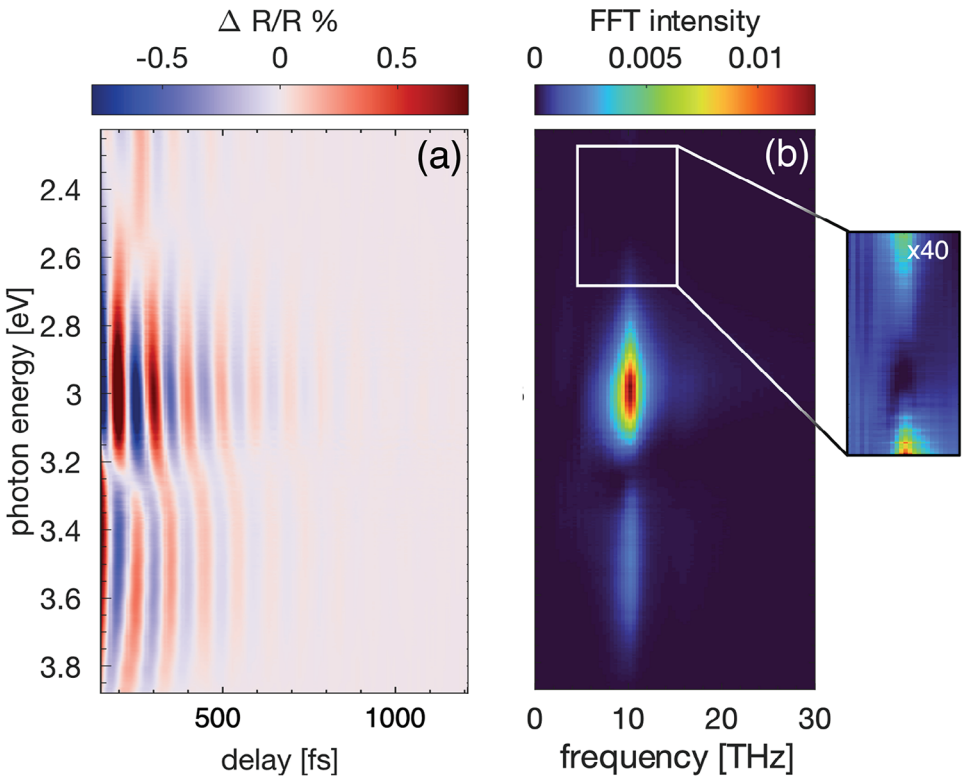

Figure 3. a) Map of the oscillatory component of the TR signal as a function of pump-probe time delay and probe photon energy after subtraction of the incoherent dynamics. b) FFT intensity map obtained from panel (a), as a function of oscillation frequency and probe photon energy. The inset reports a zoom of the FFT intensity in the region around 2.4 eV, multiplied by a factor of 40 for visibility.

one main peak centered at 10.1 THz (≈ 336 cm^{-1}). Figure 4c reports the FFT intensity as a function of probe photon energy at 10.1 THz, taken from the map in Figure 3b. Here, we notice two main peaks (at around 3 an 3.5 eV) and two regions of zero intensity, namely at around 2.45 and 3.25 eV (highlighted by light red shaded areas). Furthermore, we can study the phase of the coherent phonon being excited. The phase profile at 10.1 THz frequency is reported in Figure 4b, where two abrupt π-phase flips are clearly detected at around 2.45 and 3.25 eV (highlighted by green shaded areas).

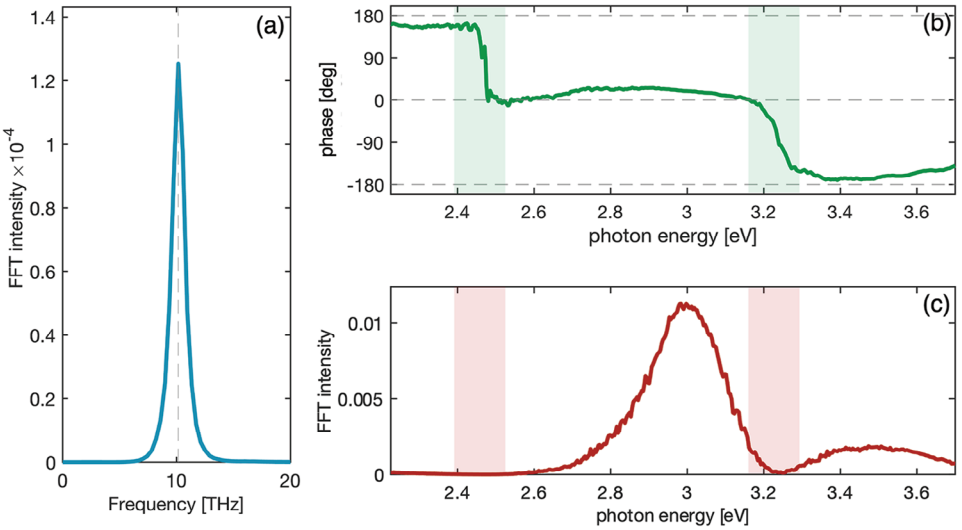

Figure 4. FFT data of the oscillatory components: a) intensity as a function of oscillation frequency for a probe photon energy of 2.64 eV; b) Phase spectral profile as a function of the probe photon energy at 10.1 THz (green shadows show the changes by π). c) intensity as a function of the probe photon energy at 10.1 THz frequency (red shadows show the regions of zero amplitude).

3. Discussion

The FFT analysis reveals one main vibrational mode at 10 THz (336 cm^{-1}), at all probe photon energies. The coherent vibrational dynamics being observed through TR spectroscopy are compatible with spontaneous Raman measurements (reported in Figure 1d), thus it is reasonable to assume that the relaxation of the Raman selection rules in the vicinity of defects is also responsible for the detection of the coherent vibrational dynamics observed in time resolved experiments, which would otherwise be optically inaccessible. It is worth mentioning that, upon photoexcitation, the excited electronic population can couple with any phonon mode within the BZ and induce coherent motion across any normal coordinate Q, depending on a momentum- and energy- specific e–ph coupling constant. However, only the subset of Raman active modes can be detected as coherent oscillations in TR signal. The relaxation of the Raman selection rules near defects is thus solely responsible for the detection of these coherent modes, while a strong coupling channel to the out-of-equilibrium electronic population is the driving force to its excitation. Moreover, in stark contrast with spontaneous Raman data, which consists of a broad, quasi-featureless band covering the entire acoustic region, the information collected from impulsive vibrational spectroscopy indicates a much more specific excitation of a single mode at 336 cm^{-1}, which we can assign to the LA branch by comparison with available literature.[14,47] More specifically, symmetry breaking induced by defects allows to detect a mode which is reminiscent of a zone edge LA phonon, as reported in both the experimental and calculated phonon dispersion relations of the material.[18,20,47] We postulate that such high specificity of the coherent response for this specific mode (among the many ones making up the broad Raman band in Figure 1d) is due to a strong coupling channel of electrons within the conduction band with the observed phonon at 10 THz. In fact, while in spontaneous Raman scattering, any Raman active phonon can scatter with light when thermally active, in coherent vibrational spectroscopy only the modes that most strongly couple with the electronic excited state are triggered coherently. This proves to be useful, as the aforementioned branch of the phonon dispersion is directly related to the phonon anomalies, which are a fingerprint of strong coupling between electrons and phonons and are closely linked to the superconducting state, according to standard BCS superconductivity.[18,21] Interestingly, the coherent activation of the mode at 10 THz seems to be rather insensitive to the kind and amount of defects in the film, which mostly play a role in making the mode Raman active, thus detectable if coherently excited. In the Supporting Information, we report TR measurements of a titanium oxynitride (TiO_xN_y) film. The static Raman spectrum has noticeable differences with respect to the one of the TiN film and boasts a much stronger scattering from higher frequency modes from the optical branches of the phonon dispersion relation. If the nature or amount of defects had a relevant influence on e–ph coupling, we would expect to see other modes being activated coherently, whereas the coherent vibrational spectrum is still dominated by the 10 THz component. This can only be attributed to a remarkable scattering channel of electrons with zone edge phonons within the LA branch.

Now the primary goals of our study are to estimate the coupling of the vibrational degrees of freedom to the electronic states, and to identify their contribution to the modulation of optical properties. Moreover, we seek a phenomenological yet physically sound description of the excitation mechanism causing the observed vibrational coherence. To this purpose we start analyzing the π phase flips observed at 2.45 and 3.25 eV. We first note that the TR signal is related to the modulation of the electronic susceptibility here caused by the driven vibrational mode. The discussed phase is thus associated with the complex susceptibility tensor. Here, we notice that these energy values are close to interband transitions reported for TiN.[57] This suggests a modulation of optical transitions as the onset of the vibrational coherence. Indeed, within a simple deformation potential scheme, one can assume that the activation of a given coherent mode of the lattice will alter the crystal field, leading to a modulation of the electronic states and a change in the cross-section of the accessible optical transitions. In particular, the periodic opening and closing of the optical gaps, induced by the coherent phonons, leads to an alternating blueshift/redshift of the optical absorption. As a result, the TR signal at probe photon energies adjacent to the static optical gap (red and blue sides) oscillates; moreover, the red side and the blue side have opposite sign, that is they are in anti-phase, giving rise to a phase difference of π across the energy corresponding to interband transition.[31] Contrary to the incoherent optical response, where only one zero crossing of the signal is present at around 3.1 eV, the coherent response shows two zero crossings, where the phase flips are found, in the vicinity of two interband transitions. This can be explained in terms of the driving force of the two TR signals. The vibrational coherence affects both optical transitions (at 3.2 and 2.45 eV) by the coupling of the phonon mode to the electronic states involved in both resonances. On the other hand, the incoherent response is caused by redistribution of the electronic density of states after the Fermi smearing and affects the probability of interband and intraband transitions in the vicinity of the Fermi level, mostly in the higher photon energy range. No relevant spectral feature nor a zero crossing is present at 2.4 eV, which means that this optical transition is left practically unaffected by the Fermi smearing within the CB. According to this picture of optical gap modulation, the nodes in the amplitude profile of the coherent TR signal are expected in the vicinity of the transition energy. Similarly, at these photon energies phase flips are present in the coherent oscillations (Figure 4c,b, respectively). A schematic representation of this process is proposed in Figure 2d. We further note that, although the discussed transitions have a relatively low oscillator strength,[4] the phase flip is very evident. Thus, our analysis allows to identify the allowed optical transitions of this material with unprecedented sensitivity, even when said transitions are superimposed to giant, metallic Drude-like contribution given by free carrier absorption. It is worth mentioning that beyond this simple physical picture, the specific amplitude of the coherent oscillations observed optically, at a given photon energy, depends on the value of the Raman tensor and on the photon energy. Moreover, the model of a Lorentzian-shaped absorption whose resonance is modulated by the phonon should include other phenomena occurring at the same time, such as the change in optical absorption induced by the Fermi smearing, both on interband and intraband absorption. Finally, the link between the phonon-induced variation in absorption and the TR signal is not immediate, as discussed below.

We also notice that the modulation of the optical gap leads to a zero-crossing point, where the TR signal remains zero. In Figure 3a the zero signal, corresponding to a zero-crossing position, appears as white. Here, we can notice that this zero-crossing position changes in time. In Figure 2e, we plot the corresponding zero-crossing position as a function of time. This allows us to provide a semi-quantitative estimation of the entity of the energy modulation of the electronic states. Since along the zero-crossing line no change in reflectivity is recorded, it is safe to assume that it correlates with the time behavior of the Fermi level of the system, whose occupation remains unvaried during the experiment. In our case, the time behavior of the zero-crossing line consists of two contributions: i) a step-like function at $t = 0$ from 3 to 2.95 eV, which is due to a small bandgap renormalization due to the change in electronic distribution within the conduction band, ii) oscillations with the same period as the coherent mode. This second term directly correlates with the modulation of the Fermi level induced by the vibrational coherence, which is expected to be close in value to the energy modulation of the optical gaps by e–ph coupling. The amplitude of this modulation is found to be of the order of 100 meV (see Figure 2e).

In order to justify the excitation mechanism of the coherent lattice motion observed in the experiments, we resolve to phenomenological models in the literature. One of such models is commonly referred as DECP, whose premise is the indirect excitation of a totally symmetric coherent phonon by means of a real excited state electronic population of limited lifetime τ_e, and entirely described by a collective variable such as the photo-excited state carrier density $n_e(t)$ or the electronic temperature associated to the excited state Fermi-Dirac distribution $T_e(t)$, interacting with the lattice through e–ph coupling.[37] The coupling of the electronic population to the lattice degrees of freedom is treated linearly, assuming the force F_Q acting on the harmonic oscillator of normal coordinate Q to be proportional to the change in $T_e(\tau)$ or $n_e(\tau)$.[27] The model assumes a simple driven-damped harmonic oscillator:

$$\mu^*\left(\frac{\partial^2 Q(t)}{\partial t^2} + 2\gamma\frac{\partial Q(t)}{\partial t} + \omega_0^2 Q(t)\right) = F_Q(t) \tag{1}$$

with μ^* being the normalized mass of the mode, γ the phonon dephasing rate (due to phonon–phonon and phonon-defect interaction, and to a decrease in the population of the given vibrational mode), ω_0 the frequency of the vibrational mode. Since the pump pulse photon energy lies within the plasmonic window of the material, we assume a purely intraband excitation of carriers within the partially filled conduction band, and we associate the driving force of the phonon oscillator exclusively to the variation in electronic temperature $\Delta T_e(t)$. We assume the following temporal dynamics for $\Delta T_e(t)$:

$$\Delta T_e(t) = e^{-\beta t} + \Delta T_e(\infty) \tag{2}$$

where β is the typical e–ph scattering rate, i.e., the inverse of the characteristic e–ph scattering time. $\Delta T_e(\infty)$ describes the electronic temperature after the complete thermalization with the lattice, and is assumed as a free parameter of the final fit. The expression of the TR calculated from the DECP model is reported in Equation (3):

$$\frac{\overline{\Delta R(t)}}{R} = A\int_0^\infty \mathrm{IRF}(t-t')\Delta T_e(t')dt' + B\frac{\omega_0^2}{\omega_0^2+\beta^2-2\gamma\beta}$$
$$\int_0^\infty \mathrm{IRF}(t-t')\left[\Delta T_e(t') - e^{-\gamma t'}\left(\cos(\Omega t') - \frac{\beta'}{\Omega}\sin(\Omega t')\right)\right]dt' \tag{3}$$

where A and B are constant factors, $\Omega = \sqrt{\omega_0^2 - \gamma^2}$ is the renormalized phonon frequency, and $\beta' = \beta - \gamma$. The result thus is found to depend on the e–ph scattering rate β and the phonon dephasing rate γ. We retrieve these parameters by performing fits of the experimental data. In particular, we use a single exponential with an added constant (similar to Equation (2) describing the dynamics of the electronic temperature) to fit the incoherent dynamics at a single photon energy and retrieve a typical e–ph scattering time of $\tau_{e-ph} = 60$ fs. On the other hand, we fit the oscillatory data with a damped harmonic oscillator to retrieve a phonon dephasing time of $\tau_{ph} = 250$ fs. These typical times are the inverse of β and γ, respectively. We then use these values as fixed coefficients in Equation (3), while leaving A, B, and $\Delta T_e(\infty)$ as free fitting parameters. The instrumental response function (IRF) is assumed to be Gaussian and is also obtained by fitting the experimental data. It is noteworthy that the initial phase of the coherent oscillations is given by:

$$\tan(\phi_0) = \frac{\beta'}{\Omega} = \frac{\beta-\gamma}{\Omega} = \frac{\beta-\gamma}{\sqrt{\omega_0^2-\gamma^2}} \tag{4}$$

and is solely dependent on the phonon frequency, the phonon dephasing rate, and the e–ph scattering rate. Hence, in the limit of an electronic excited state lifetime much longer than the phonon lifetime, the excitation is quasi-displacive with a cosine-like oscillation, while in the opposite limit case the excitation can be considered quasi-impulsive with a sine-like oscillation behavior.[58] In **Figure 5a**, we show a representative case (probe photon energy set at 2.64 eV) of experimental data with DECP fitting. We highlight that, since ω_0, β, and γ, are fixed values, the initial phase ϕ_0 of the oscillations is not a free parameter of the fit, and is determined by these three parameters, as shown in Equation (4). Note that the DECP model (Figure 5a) perfectly matches the oscillations in the experimental data, with the correct phase. This serves as an excellent validation of the DECP model as a description of the physical process underlying the generation of the observed vibrational coherence. We expect similar results for any probe photon-energy, with flips in sign of the TR oscillations, depending on the crossing on an electronic resonance, taken into account by the B term.[37]

The broadband detection scheme of the experiments also allows to analyze the spectral profile of the oscillation amplitude across the entire visible-near UV range. According to a simple first order approach, we can write the expected oscillation amplitude at different probe photon energies. In particular, we expand the phonon-related modulation depth in reflectivity ΔR to the first order in the normal mode coordinate Q, by taking into

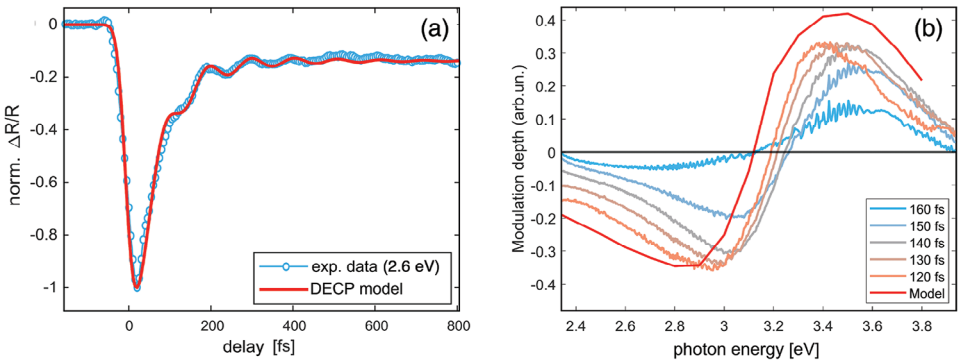

Figure 5. a) TR temporal behavior (at 2.64 eV probe photon energy): experimental data (blue circles) and fit by DECP model (red line). b) Modulation amplitude as a function of the probe photon-energy: experimental data for various time delays (in the legend) and data from the model (red line).

account the modulation in optical susceptibility χ induced by the phonon mode (i.e., the Raman tensor), and we get:

$$\Delta R \sim \frac{\partial R}{\partial \chi}\frac{\partial \chi}{\partial Q}Q \tag{5}$$

By further expanding the differential reflectivity ΔR, the following expression is obtained:[59]

$$\Delta R = \left|\frac{\partial(\chi_1 + i\chi_2)}{\partial Q}\right|\left(\frac{\partial R}{\partial \chi_1}\cos(\eta) + \frac{\partial R}{\partial \chi_2}\sin(\eta)\right) \times Q \tag{6}$$

where the first term $\Re(\omega) = \left|\partial\left(\chi_1(\omega) + i\chi_2(\omega)\right)/\partial Q\right|$ is a complex tensorial quantity, reminiscent of a Raman tensor, while η is the phase of $\Re(\omega)$. The ab initio calculation of this quantity is not immediate, as it requires to retrieve the optical susceptibility at varying Q by means of frozen phonon calculation, as was done in several recent works.[60] Nevertheless, from the theory of electronic (resonant) Raman scattering, it can be verified that for two band contributions, second order perturbation theory predicts that in the vicinity of an electronic resonance, the Raman tensor is simply proportional to the derivative of the susceptibility with respect to the exciting photon frequency, $\frac{\partial \chi}{\partial Q} \sim \frac{\partial \chi}{\partial \omega}$.[61] We access to this quantity from spectrometric ellipsometry, reported in Figure 1b. A direct comparison of the expected modulation depth with the experimental amplitude of the oscillating residuals (which are only related to the contribution from vibrational coherence), is reported in Figure 5b. Comparing the experimental spectra of the oscillating residuals at varying delays (orange to blue lines) with the model curve (red line), we observe that the model well matches the experimental behavior, including the change in sign at around 3–3.2 eV discussed above. The change in the spectral position of the zero-crossing point at increasing time delays is not captured; nevertheless, this is expected, as it is likely due to bandgap renormalization whose driving force is solely related to the electronic distribution, as already discussed, which is not entailed by Equation (5). Finally, it is worth mentioning that the observed phenomena can find technological applications in all-optical modulators: as a matter of fact, the induced oscillations in the optical response can be not only very fast, but also strong enough to exceed the background incoherent signal. In particular, note that at probe photon energies far from optical absorption the coherent signal can be higher than the incoherent by more than a factor of two (see Figure S4, Supporting Information). We also expect this behavior to be enhanced by shaped or multiple excitation pulses.[62–64]

4. Conclusion

We studied the real-time coherent vibrational dynamics in TiN through femtosecond broadband transient reflection spectroscopy. We demonstrate that the intraband excitation of free carriers in the conduction band of TiN by femtosecond pulses allows to coherently excite the lattice degrees of freedom. The presence of defects and nonstoichometries in the TiN lattice allows for a relaxation of the Raman selection rules (i.e., a local nonzero Raman tensor), thus enabling the all-optical detection of otherwise optically inactive coherent (local) modes, also from points far from the BZ center.

In particular, the local mode being detected in time-resolved experiments is related to zone-edge phonons within the LA branch, which contains several fingerprints of strong coupling between electrons and phonons and is closely linked to the superconducting state. This appears useful for providing an accurate benchmarking of the coherent response of strongly coupled systems, in the quest for nonlinear, time-resolved techniques to apply to more complex systems, such as nonconventional superconductors.[65]

The accurate study of the amplitude and phase profiles across the probe photon energy range allows to disentangle the coupling of the coherent phonon to electronic optical transitions. In particular, the coherent onset of lattice motion induces a modulation of the binding energy, and electronic bands by as much as 100 meV.

Moreover, thanks to the sensitivity of the coherent response to the change in optical gaps, we achieve unmatched precision for the detection of interband transitions that would be impossible to obtain through common static spectroscopy, where, for prominently metallic materials, the resonant interband terms of the Drude-Lorentz model are hidden by an intense Drude-like contribution from the free carrier absorption.[31]

We finally provide a complete phenomenological characterization of the observed coherent dynamics within the framework of DECP theory, and draw definitive conclusions on the nature of the excitation mechanism as being mediated by a hot electron distribution, and driven by e–ph coupling.

5. Experimental Methods

Sample Preparation: The sample was deposited via PLD on a fused silica substrate that was previously cleaned with isopropanol in an ultrasonic bath. The ablation of a high purity (99.9% Mateck Gmbh) TiN target was achieved through the use of a Q-switched Nd:YAG ns pulsed laser, whose frequency was doubled through second harmonic generation, thus providing a central wavelength $\lambda = 532$ nm. The pulse duration was ≈6 ns, the repetition rate 10 Hz, while the fluence was set at 1.7 J · cm^{-2}. The deposition occurs in vacuum ($4 \cdot 10^{-4}$ Pa). The sample was placed at a distance of 50 mm from the target, the sample was rotated by a stepper motor. To ensure high crystalline order, a subsequent annealing treatment was performed in a reducing environment of H_2/N_2 gas, at 823 K and small overpressure, for 3 h. The morphology and the thickness of the film was assessed through field emission scanning electron microscopy (SEM, Zeiss SUPRA 40). Static reflectance and transmittance measurements were performed via a Perkin Elmer Lambda 1050 spectrometer, equipped with a 150-mm diameter Spectralon-coated integrating sphere. The absorbance was retrieved according to the formula 1-T-R. Ellipsometric measurements were provided by variable-angle spectroscopic ellipsometry (V-VASE) in the range of 0.6–6.5 eV and an energy interval of 0.1 eV at 65° and 75° angles of incidence, with a J.A. Woollam NIR-UV VASE. Raman spectra were collected by a Renishaw InVia micro-Raman spectrometer with excitation by an argon ion laser ($\lambda = 514$ nm, green) with the laser power reaching the sample fixed at 0.13 mW to minimize the probability of sample damage by the laser.

Transient Reflectivity Measurements: The pump-probe setup employed was based on a chirped-pulse amplified Ti:sapphire laser, delivering 100 fs pulses at 800 nm central wavelength and operating at 2 kHz repetition rate. The pump beam was generated through a noncollinear optical parametric amplifier (NOPA), providing broadband (100 nm FWHM) tunable pulses over the entire visible range (490–750 nm). The pulses were then compressed by means of a chirped mirror pair, allowing to reach a temporal duration of less than 15 fs. Temporal characterization of the pump pulses was performed through sum frequency generation frequency resolved optical gating (SFG-FROG). The pump fluence was set to 1.4 mJ cm^{-2}. The probe pulses consisted of a white light supercontinuum generated by focusing the fundamental of the Ti:sapphire system on a CaF_2 plate having a thickness of 3 mm. Both the pump and probe pulses were focused on the sample at near normal incidence. The reflection of the probe was dispersed by a grating and collected by an optical multichannel analyzer (Princeton Instruments Ltd.), allowing to spectrally resolve the probe. An electronically controlled stage on the probe optical path varies the delay between pump and probe pulses. In order to minimize fluctuations in laser intensity, the differential reflectivity signal was measured stroboscopically, i.e., the reflectivity of the unperturbed and photoexcited sample were collected for two consecutive probe pulses of the Ti:sapphire system, in absence and in presence of the pump pulse, respectively. The polarization directions of pump and probe beams were kept orthogonal so as to reduce scattering artifacts. The TR spectra were dechirped with a third order polynomial, to take into account the dispersion of the probe beam. Since the temporal dynamics were comprised of both an incoherent contribution and a set of coherent oscillations, the incoherent part of the signal was subtracted through unconstrained biexponential fitting, convoluted with a Gaussian-shaped IRF. The detection of the time-zero (i.e., the temporal overlap between pump and probe pulses at each wavelength) was performed from the IRF fitting results.

Supporting Information

Supporting Information is available from the Wiley Online Library or from the author.

Acknowledgements

A.I. and G.C. acknowledged financial support by the European Union's NextGenerationEU Programme with the IPHOQS Infrastructure [IR0000016, ID D2B8D520, CUP B53C22001750006] "Integrated Infrastructure Initiative in Photonic and Quantum Sciences". C.M. and A.L.B. acknowledged partial funding by the National Recovery and Resilience Plan (NRRP), Mission 4 Component 2 Investment 1.3-Call for tender No. 1561 of 11.10.2022 of Ministero dell'Università e della Ricerca (MUR); funded by the European Union-NextGenerationEU. Award project code PE0000021, Concession Decree No. 1561 of 11.10.2022 adopted by MUR, CUP D43C22003090001, Project title "Network 4 Energy Sustainable Transition-NEST". L. M. acknowledged the support from the funding from Czech Science Foundation (GACR) through the project 21-05259S and from the Ministry of Education, Youth, and Sports of the Czech Republic, CAAS - Project Center of Advanced Applied Sciences, project number: CZ.02.1.01/0.0/0.0/16 019/0000778 (European Structural and Investments Funds – Operational Programme Research, Development, and Education). Spectroscopic ellipsometry experiments were performed at the CzechNanoLab Research Infrastructure supported by the Ministry of Education,Youth and Sport of the Czech Republic (grant LM2023051). A.N. acknowledged financial support by the European Union-NextGenerationEU Programme, the National Recovery and Resilience Plan (NRRP), Mission 4 Component 2 Investment 1.1 PRIN 2022 PNRR, Ministero dell'Universitè e della Ricerca (MUR), CUP D53D23017090001, ID P2022J5NAN "Refractory plasmonic metasurfaces for solar thermal catalytic CO2 conversion" (RESOLCAT). M.Z.-R. acknowledged financial support by the European Union-NextGenerationEU Programme, the National Recovery and Resilience Plan (NRRP), Mission 4 Component 2 Investment 1.1 PRIN 2022 PNRR Ministero dell'Universitè e della Ricerca (MUR), CUP D53D23019400001, ID P2022RL4TR "All-oxide nanowire plasmonic solar cells (NanoSolar)."

Open access publishing facilitated by Politecnico di Milano, as part of the Wiley - CRUI-CARE agreement.

Conflict of Interest

The authors declare no conflict of interest.

Data Availability Statement

The data that support the findings of this study are available from the corresponding author upon reasonable request.

Keywords

coherent phonons, e–ph coupling, plasmonics, titanium nitride, ultrafast spectroscopy

Received: May 22, 2024
Revised: August 26, 2024
Published online:

[1] P. Patsalas, S. Logothetidis, *J. Appl. Phys.* **2001**, *90*, 4725.
[2] M. Dasog, *Chem. Mater.* **2022**, *34*, 4249.
[3] G. V. Naik, J. L. Schroeder, X. Ni, A. V. Kildishev, T. D. Sands, A. Boltasseva, *Opt. Mater. Express* **2012**, *2*, 478.
[4] P. Patsalas, N. Kalfagiannis, S. Kassavetis, *Materials* **2015**, *8*, 3128.
[5] C. M. Zgrabik, E. L. Hu, *Opt. Mater. Express* **2015**, *5*, 2786.
[6] A. Kharitonov, S. Kharintsev, *Opt. Mater. Express* **2020**, *10*, 513.
[7] P. Patsalas, N. Kalfagiannis, S. Kassavetis, G. Abadias, D. V. Bellas, C. Lekka, E. Lidorikis, *Mater. Sci. Eng.: R: Rep.* **2018**, *123*, 1.
[8] S. Molesky, C. J. Dewalt, Z. Jacob, *Opt. Express* **2013**, *21*, A96.
[9] A. Naldoni, Z. A. Kudyshev, L. Mascaretti, S. P. Sarmah, S. Rej, J. P. Froning, O. Tomanec, J. E. Yoo, D. Wang, t. Kment, T. Montini, P. Fornasiero, V. M. Shalaev, P. Schmuki, A. Boltasseva, R. Zbořil, *Nano Lett.* **2020**, *20*, 3663.

[10] S. Saha, A. Dutta, N. Kinsey, A. V. Kildishev, V. M. Shalaev, A. Boltasseva, *ACS Photonics* **2018**, *5*, 4423.
[11] N. Sun, D. Zhou, W. Liu, A. Li, Y. Su, P. Jiang, Y. Zou, S. Shi, F. Liu, *J. Power Sources* **2021**, *489*, 229406.
[12] A. Naldoni, U. Guler, Z. Wang, M. Marelli, F. Malara, X. Meng, L. V. Besteiro, A. O. Govorov, A. V. Kildishev, A. Boltasseva, V. M. Shalaev, *Adv. Opt. Mater.* **2017**, *5*, 1601031.
[13] H. Reddy, U. Guler, Z. Kudyshev, A. V. Kildishev, V. M. Shalaev, A. Boltasseva, *ACS Photonics* **2017**, *4*, 1413.
[14] S. Dal Forno, J. Lischner, *Physical Review Materials* **2019**, *3*, 115203.
[15] B. T. Diroll, S. Saha, V. M. Shalaev, A. Boltasseva, R. D. Schaller, *Adv. Opt. Mater.* **2020**, *8*, 2000652.
[16] T. Reese, A. N. Reed, A. D. Sample, F. Freire-Fernández, R. D. Schaller, A. M. Urbas, T. W. Odom, *ACS Photonics* **2021**, *8*, 1556.
[17] S. Rotta Loria, B. R. Bricchi, A. Schirato, L. Mascaretti, C. Mancarella, A. Naldoni, A. Li Bassi, G. Della Valle, M. Zavelani-Rossi, *Adv. Opt. Mater.* **2023**, *11*, 2300333.
[18] W. Kress, P. Roedhammer, H. Bilz, W. D. Teuchert, A. N. Christensen, *Phys. Rev. B* **1978**, *17*, 111.
[19] B. Sacépé, C. Chapelier, T. I. Baturina, V. M. Vinokur, M. R. Baklanov, M. Sanquer, *Nat. Commun.* **2010**, *1*, 140.
[20] E. Isaev, S. Simak, I. Abrikosov, R. Ahuja, Y. Kh. Vekilov, M. Katsnelson, A. Lichtenstein, B. Johansson, *J. Appl. Phys.* **2007**, *101*, 123519.
[21] W. Hanke, J. Hafner, H. Bilz, *Phys. Rev. Lett.* **1976**, *37*, 1560.
[22] W. Weber, *Phys. Rev. B* **1973**, *8*, 5093.
[23] S. L. Johnson, *Faraday Discuss.* **2022**, *237*, 9.
[24] C. Giannetti, M. Capone, D. Fausti, M. Fabrizio, F. Parmigiani, D. Mihailovic, *Adv. Phys.* **2016**, *65*, 58.
[25] D. Juraschek, M. Fechner, N. Spaldin, *Phys. Rev. Lett.* **2017**, *118*, 054101.
[26] M. Mitrano, A. Cantaluppi, D. Nicoletti, S. Kaiser, A. Perucchi, S. Lupi, P. Di Pietro, D. Pontiroli, M. Riccò, S. R. Clark, D. Jaksch, A. Cavalleri, *Nature* **2016**, *530*, 461.
[27] F. Giorgianni, M. Udina, T. Cea, E. Paris, M. Caputo, M. Radovic, L. Boie, J. Sakai, C. W. Schneider, S. L. Johnson, *Commun. Phys.* **2022**, *5*, 1.
[28] M. Först, C. Manzoni, S. Kaiser, Y. Tomioka, Y. Tokura, R. Merlin, A. Cavalleri, *Nat. Phys.* **2011**, *7*, 854.
[29] T. Y. Jeong, B. M. Jin, S. H. Rhim, L. Debbichi, J. Park, Y. D. Jang, H. R. Lee, D.-H. Chae, D. Lee, Y.-H. Kim, S. Jung, K. J. Yee, *ACS Nano* **2016**, *10*, 5560.
[30] C. Trovatello, H. P. C. Miranda, A. Molina-Sánchez, R. Borrego-Varillas, C. Manzoni, L. Moretti, L. Ganzer, M. Maiuri, J. Wang, D. Dumcenco, A. Kis, L. Wirtz, A. Marini, G. Soavi, A. C. Ferrari, G. Cerullo, D. Sangalli, S. D. Conte, *ACS Nano* **2020**, *14*, 5700.
[31] C. J. Sayers, S. Dal Conte, D. Wolverson, C. Gadermaier, G. Cerullo, E. Carpene, E. Da Como, *Adv. Opt. Mater.* **2022**, *10*, 2200362.
[32] C. J. Sayers, H. Hedayat, A. Ceraso, F. Museur, M. Cattelan, L. S. Hart, L. S. Farrar, S. Dal Conte, G. Cerullo, C. Dallera, E. Da Como, E. Carpene, *Phys. Rev. B* **2020**, *102*, 161105.
[33] J. Fu, M. Li, A. Solanki, Q. Xu, Y. Lekina, S. Ramesh, Z. X. Shen, T. C. Sum, *Adv. Mater.* **2021**, *33*, 11.
[34] G. Kaur, A. Shukla, K. Justice Babu, H. N. Ghosh, *ACS Photonics* **2022**, *9*, 2756.
[35] F. Thouin, D. A. Valverde-Chávez, C. Quarti, D. Cortecchia, I. Bargigia, D. Beljonne, A. Petrozza, C. Silva, A. R. Srimath Kandada, *Nat. Mater.* **2019**, *18*, 349.
[36] Y. Yan, J. Gamble, Edward B., K. A. Nelson, *J. Chem. Phys.* **1985**, *83*, 5391.
[37] H. J. Zeiger, J. Vidal, T. K. Cheng, E. P. Ippen, G. Dresselhaus, M. S. Dresselhaus, *Phys. Rev. B* **1992**, *45*, 768.
[38] T. E. Stevens, J. Kuhl, R. Merlin, *Phys. Rev. B* **2002**, *65*, 144304.
[39] D. M. Riffe, A. J. Sabbah, *Phys. Rev. B* **2007**, *76*, 085207.
[40] N. D. Lanzillotti-Kimura, K. P. O'Brien, J. Rho, H. Suchowski, X. Yin, X. Zhang, *Phys. Rev. B* **2018**, *97*, 235403.
[41] E. Baldini, T. Palmieri, A. Dominguez, P. Ruello, A. Rubio, M. Chergui, *Nano Lett.* **2018**, *18*, 5007.
[42] E. Baldini, A. Dominguez, T. Palmieri, O. Cannelli, A. Rubio, P. Ruello, M. Chergui, *Sci. Adv.* **2019**, *5*, eaax2937.
[43] J.-J. Li, K.-D. Zhu, *Phys. Rep.* **2013**, *525*, 223.
[44] M. Hase, M. Katsuragawa, A. M. Constantinescu, H. Petek, *New J. Phys.* **2013**, *15*, 055018.
[45] D. M. Juraschek, N. A. Spaldin, *Science* **2017**, *357*, 873.
[46] D. Rasic, R. Sachan, M. F. Chisholm, J. Prater, J. Narayan, *Cryst. Growth Des.* **2017**, *17*, 6634.
[47] W. Spengler, R. Kaiser, A. N. Christensen, G. Möller-Vogt, *Phys. Rev. B* **1978**, *17*, 1095.
[48] G. Benedek, G. F. Nardelli, *Phys. Rev.* **1967**, *155*, 1004.
[49] G. Benedek, G. F. Nardelli, *Phys. Rev.* **1967**, *154*, 872.
[50] G. Benedek, E. Mulazzi, *Phys. Rev.* **1969**, *179*, 906.
[51] M. Stoehr, C.-S. Shin, I. Petrov, J. E. Greene, *J. Appl. Phys.* **2011**, *110*, 083503.
[52] L. Mascaretti, T. Barman, B. R. Bricchi, F. Mönz, A. Li Bassi, t. Kment, A. Naldoni, *Appl. Surf. Sci.* **2021**, *554*, 149543.
[53] G. Della Valle, F. Scotognella, A. R. S. Kandada, M. Zavelani-Rossi, H. Li, M. Conforti, S. Longhi, L. Manna, G. Lanzani, F. Tassone, *J. Phys. Chem. Lett.* **2013**, *4*, 3337.
[54] F. Scotognella, G. Della Valle, A. R. Srimath Kandada, D. Dorfs, M. Zavelani-Rossi, M. Conforti, K. Miszta, A. Comin, K. Korobchevskaya, G. Lanzani, L. Manna, F. Tassone, *Nano Lett.* **2011**, *11*, 4711.
[55] A. Habib, F. Florio, R. Sundararaman, *J. Opt.* **2018**, *20*, 064001.
[56] A. Schirato, M. Maiuri, G. Cerullo, G. Della Valle, *Nanophotonics* **2023**, *12*, 1.
[57] K. Köhler, H. P. Geserich, T. Wolf, G. Möller-Vogt, *Phys. Status Solidi B* **1983**, *119*, 605.
[58] K. Ishioka, O. V. Misochko, in,*Progress in Ultrafast Intense Laser Science: Volume V*, (Eds.: K. Yamanouchi, A. Giulietti, K. Ledingham), Springer Series in Chemical Physics, Springer, Berlin, Heidelberg, **2010**, pp. 47–63.
[59] R. Merlin, *Solid State Commun.* **1997**, *102*, 207.
[60] C. J. Sayers, A. Genco, C. Trovatello, S. D. Conte, V. O. Khaustov, J. Cervantes-Villanueva, D. Sangalli, A. Molina-Sanchez, C. Coletti, C. Gadermaier, G. Cerullo, *Nano Lett.* **2023**, *23*, 9235.
[61] M. Cardona, G. Güntherodt, editors, *Light Scattering in Solids IV*, volume *54* of Topics in Applied Physics, Springer, Berlin, Heidelberg **1984**.
[62] O. V. Misochko, M. V. Lebedev, H. Schäfer, T. Dekorsy, *J. Phys.: Condens. Matter* **2007**, *19*, 406220.
[63] T. Dekorsky, W. Kött, T. Pfeifer, H. Kurz, *Europhys. Lett. (EPL)* **1993**, *23*, 223.
[64] T. Shimada, C. Frischkorn, M. Wolf, T. Kampfrath, *J. Appl. Phys.* **2012**, *112*, 113103.
[65] K. Ishioka, A. Pashkin, C. Bernhard, H. Petek, X. Yao, J. Demsar, *Phys. Rev. B* **2023**, *107*, 184302.